ϕ decay: A relevant source for K^- production at energies available at the GSI Schwerionen-Synchrotron (SIS)?

G. Agakishiev,[8] A. Balanda,[3,*] B. Bannier,[5] R. Bassini,[9] D. Belver,[15] A. V. Belyaev,[6] A. Blanco,[2] M. Böhmer,[11] J. L. Boyard,[13] P. Braun-Munzinger,[4,†] P. Cabanelas,[15] E. Castro,[15] S. Chernenko,[6] T. Christ,[11] M. Destefanis,[8] J. Díaz,[16] F. Dohrmann,[5] A. Dybczak,[3] T. Eberl,[11] L. Fabbietti,[11,‡] O. V. Fateev,[6] P. Finocchiaro,[1] P. Fonte,[2,§] J. Friese,[11] I. Fröhlich,[7] T. Galatyuk,[4] J. A. Garzón,[15] R. Gernhäuser,[11] A. Gil,[16] C. Gilardi,[8] M. Golubeva,[10] D. González-Díaz,[4] F. Guber,[10] M. Heilmann,[7] T. Heinz,[4] T. Hennino,[13] R. Holzmann,[4] A. Ierusalimov,[6] I. Iori,[9,‖] A. Ivashkin,[10] M. Jurkovic,[11] B. Kämpfer,[5,¶] K. Kanaki,[5] T. Karavicheva,[10] D. Kirschner,[8] I. Koenig,[4] W. Koenig,[4] B. W. Kolb,[4] R. Kotte,[5] F. Krizek,[14] R. Krücken,[11] W. Kühn,[8] A. Kugler,[14] A. Kurepin,[10] S. Lang,[4] J. S. Lange,[8] K. Lapidus,[10] T. Liu,[13] L. Lopes,[2] M. Lorenz,[7] L. Maier,[11] A. Mangiarotti,[2] J. Markert,[7] V. Metag,[8] B. Michalska,[3] J. Michel,[7] D. Mishra,[8] E. Morinière,[13] J. Mousa,[12] C. Müntz,[7] L. Naumann,[5] J. Otwinowski,[3] Y. C. Pachmayer,[7] M. Palka,[4] Y. Parpottas,[12] V. Pechenov,[8] O. Pechenova,[8] T. Pérez Cavalcanti,[8] J. Pietraszko,[4] W. Przygoda,[3,**] B. Ramstein,[13] A. Reshetin,[10] M. Roy-Stephan,[13] A. Rustamov,[4] A. Sadovsky,[10] B. Sailer,[11] P. Salabura,[3] A. Schmah,[11,††] E. Schwab,[4] Yu. G. Sobolev,[14] S. Spataro,[8] B. Spruck,[8] H. Ströbele,[7] J. Stroth,[7,4] C. Sturm,[7] M. Sudol,[13] A. Tarantola,[7] K. Teilab,[7] P. Tlusty,[14] M. Traxler,[4] R. Trebacz,[3] H. Tsertos,[12] V. Wagner,[14] M. Weber,[11] M. Wisniowski,[3] T. Wojcik,[3] J. Wüstenfeld,[5] S. Yurevich,[4] Y. V. Zanevsky,[6] P. Zhou,[5] and P. Zumbruch[4]

(HADES Collaboration)

[1]*Istituto Nazionale di Fisica Nucleare-Laboratori Nazionali del Sud, I-95125 Catania, Italy*

[2]*LIP-Laboratório de Instrumentação e Física Experimental de Partículas, 3004-516 Coimbra, Portugal*

[3]*Smoluchowski Institute of Physics, Jagiellonian University of Cracow, PL-30-059 Kraków, Poland*

[4]*GSI Helmholtzzentrum für Schwerionenforschung GmbH, D-64291 Darmstadt, Germany*

[5]*Institut für Strahlenphysik, Forschungszentrum Dresden-Rossendorf, D-01314 Dresden, Germany*

[6]*Joint Institute of Nuclear Research, RU-141980 Dubna, Russia*

[7]*Institut für Kernphysik, Johann Wolfgang Goethe-Universität, D-60438 Frankfurt, Germany*

[8]*II. Physikalisches Institut, Justus Liebig Universität Giessen, D-35392 Giessen, Germany*

[9]*Istituto Nazionale di Fisica Nucleare, Sezione di Milano, I-20133 Milano, Italy*

[10]*Institute for Nuclear Research, Russian Academy of Science, RU-117312 Moscow, Russia*

[11]*Physik Department E12, Technische Universität München, D-85748 München, Germany*

[12]*Department of Physics, University of Cyprus, 1678 Nicosia, Cyprus*

[13]*Institut de Physique Nucléaire (UMR 8608), CNRS/IN2P3-Université Paris Sud, F-91406 Orsay Cedex, France*

[14]*Nuclear Physics Institute, Academy of Sciences of Czech Republic, 25068 Rez, Czech Republic*

[15]*Departamento de Física de Partículas, Universidad de Santiago de Compostela, 15706 Santiago de Compostela, Spain*

[16]*Instituto de Física Corpuscular, Universidad de Valencia-CSIC, 46971 Valencia, Spain*

(Received 9 March 2009; published 26 August 2009)

We present phase space distributions and multiplicities of K^+, K^-, and ϕ mesons produced in Ar + KCl reactions at a kinetic beam energy of 1.756 GeV/nucleon and measured with the HADES spectrometer. The inverse slope parameters and yields of kaons supplement the systematics of previous measurements. The percentage of K^- mesons coming from ϕ decay is found to be $18 \pm 7\%$.

DOI: 10.1103/PhysRevC.80.025209 PACS number(s): 25.75.Dw, 13.25.Gv

I. INTRODUCTION

The systematic study of $K^\pm$ subthreshold production yields, phase space distributions, and flow observables in relativistic heavy-ion collisions at various beam energies and for various system sizes and centralities has attracted much attention, in particular in the context of in-medium properties of K^+ and K^- mesons [1–10]. Corresponding experiments have been the focus of studies by the KaoS [11–15] and FOPI [16–20] Collaborations over the last two decades, following up on the pioneering experiments at Bevalac [21]. The heavy-ion data are supplemented by proton-induced reactions on nuclei [22, 23] with measurements of inclusive K^+ and K^- production. Concerning the elementary proton-proton reactions, the recent measurements by the COSY-11 [24], TOF [25], and ANKE [26,27] Collaborations provided valuable reference data.

High statistics data for K^+ production allowed conclusions on the K^+-nucleon potential and on the nuclear equation of

[*]Also at Panstwowa Wyzsza Szkola Zawodowa, 33-300 Nowy Sacz, Poland.

[†]Also at Extreme Matter Institute, GSI Helmholtzzentrum für Schwerionenforschung, D-64291, Germany.

[‡]Corresponding author: laura.fabbietti@ph.tum.de; also at Excellence Cluster Universe, Technische Universität München, Boltzmannstr.2, D-85748, Garching, Germany.

[§]Also at ISEC Coimbra, Coimbra, Portugal.

[‖]Also at Dipartimento di Fisica, Universitá di Milano, 20133 Milano, Italy.

[¶]Also at Technische Universität Dresden, 01062 Dresden, Germany.

[**]Also at Panstwowa Wyzsza Szkola Zawodowa, 33-300 Nowy Sacz, Poland.

[††]Corresponding author: alexander.schmah@ph.tum.de; also at Excellence Cluster Universe, Technische Universität München, Boltzmannstr.2, D-85748, Garching, Germany.

state [11,13] to be drawn. From the analysis of the out-of-plane [28,29] and sideward flow [19,30], the K^+-nucleon potential is deduced to be mildly repulsive, and the measured K^+ production yields are in agreement with the scenario of a soft nuclear equation of state (incompressibility modulus $K_N \approx 200$ MeV) [31,32]. The interpretation of the K^- data is still undergoing systematic evaluations to pin down the value of the presumed attractive K^--nucleon potential and its momentum dependence.

Recent data [15] have contributed to our understanding of the production mechanism of $K^\pm$ mesons. Indeed, the combined analysis of K^+ and K^- suggests that a substantial part of the observed K^- mesons is due to a strangeness exchange mechanism [33]. Furthermore K^+ and K^- exhibit distinctively different in-medium properties, both in theoretical approaches [1–10,31–34] and in experiments [11–13,15,18,19,22].

The spectrometer HADES [35], primarily designed to measure di-electrons [36], has been recently employed for the identification of strange mesons as well, showing high purity and efficiency for particle identification and excellent reconstruction capability of secondary decay vertices [37]. For the first time, a combined and inclusive identification of K^+, K^-, and ϕ mesons was carried out in the same experimental setup at a subthreshold beam energy. ("Subthreshold" refers to free nucleon-nucleon collisions and applies here to the K^- and ϕ channels.) Our measurement allows firm conclusions on the fraction of K^- mesons that originate from the ϕ decay. It is argued in Ref. [38] that, if a substantial part of the observed K^- stems from ϕ decays, the interpretation of data in terms of a strongly reduced effective antikaon mass in the nuclear medium needs a proper account of this channel. Indeed, the data in Ref. [20], unfortunately hampered by poor statistics, gave one of the first indications of the importance of K^- feeding from ϕ decays. Here, we report on the phase space distributions and yields of $K^\pm$ and ϕ mesons in the reaction Ar + KCl at a kinetic beam energy of 1.756 GeV/nucleon. We provide an estimate of the feeding contribution of ϕ decays to the K^- abundance. Our article is organized as follows. Section II describes the experiment and Sec. III is devoted to the data analysis. Experimental results on transverse mass spectra, rapidity distributions, and multiplicities of $K^\pm$ and ϕ mesons are presented in Sec. IV. Our findings are discussed in Sec. V and summarized in Sec. VI.

II. THE EXPERIMENT

The experiment was performed with the High Acceptance Di-Electron Spectrometer HADES at the heavy-ion synchrotron SIS at GSI Helmholtzzentrum für Schwerionenforschung in Darmstadt, Germany. A detailed description of the spectrometer is presented in Ref. [35]. In the following we summarize the main features of the apparatus. HADES consists of a six-coil toroidal magnet centered on the beam axis and six identical detection sections located between the coils and covering polar angles from 18° to 85°. In the measurement presented here, the six sectors comprised a gaseous ring-imaging Cherenkov (RICH) detector, four planes of multiwire drift chambers (MDCs) for track reconstruction, and two time-of-flight walls (TOF and TOFino), supplemented at forward polar angles with pre-shower chambers. In the outermost plane, two opposite MDCs were not installed, and they were not used for $K^\pm$ identification. For each sector, the TOF and TOFino/pre-shower detectors were combined into META (multiplicity and electron trigger array) detectors.

An $^{40}_{18+}$Ar beam of $\sim 10^6$ particles/s was incident on a fourfold segmented KCl target with a total thickness corresponding to 3.3% interaction length. A fast diamond start detector located upstream of the target was used to determine the interaction time. The data readout was started by a first-level trigger (LVL1) decision, requiring an observed charged particle multiplicity MUL $\geqslant 18$ in the TOF/TOFino detectors, accepting approximately 35% of the nuclear reaction cross section. It was followed by a second-level trigger (LVL2) requesting at least one $e^\pm$ hit in the RICH detector per event. This selection, however, has not introduced any bias into the hadron analysis. A fraction of 10% of the LVL1 triggered events was stored regardless of the LVL2 condition. Comparison between the pure LVL1 and the LVL1 + LVL2 events showed only insignificant differences in the total track multiplicity and hence the centrality of the reaction.

III. DATA ANALYSIS

A. Track reconstruction

A reconstructed hadron track in the spectrometer is composed of inner and outer track segments in the MDCs that define straight lines between the first two MDC planes, the last two MDC planes behind the magnet, and a hit point in one of the META detectors. In the so-called cluster finder [35,39] and track-segment fitting procedures possible trajectories through the MDC segments are calculated. The pointing vector of the outer track segment was used for matching the META hit to the MDC track segments, generating a track candidate. A Runge-Kutta algorithm was implemented for calculating the momentum of each of the track candidates by solving the equation of motion inside the magnetic field region [40]. The quality of the META hit-matching procedure and the quality of the Runge-Kutta fitting (characterized by χ^2 values) are used to create a list of ordered track candidates. To resolve matching ambiguities, only the track candidate with the smallest value of the product of the two χ^2 values is declared a true track. Its components and associated track candidates are deleted from the candidate list. This procedure is repeated until no more track candidates are left in the list.

B. Particle identification

Because the RICH detector is only used to distinguish $e^\pm$ from hadrons, this system is not employed in the following analysis, which deals exclusively with hadron reconstruction. Hence, only the time-of-flight walls TOF and TOFino + Pre-Shower (this detector is used to refine the position of the TOFino hits) and the MDCs are used to identify hadrons.

The particles can be distinguished by their velocity and by their energy loss (dE/dx). The particle velocity β (in units of

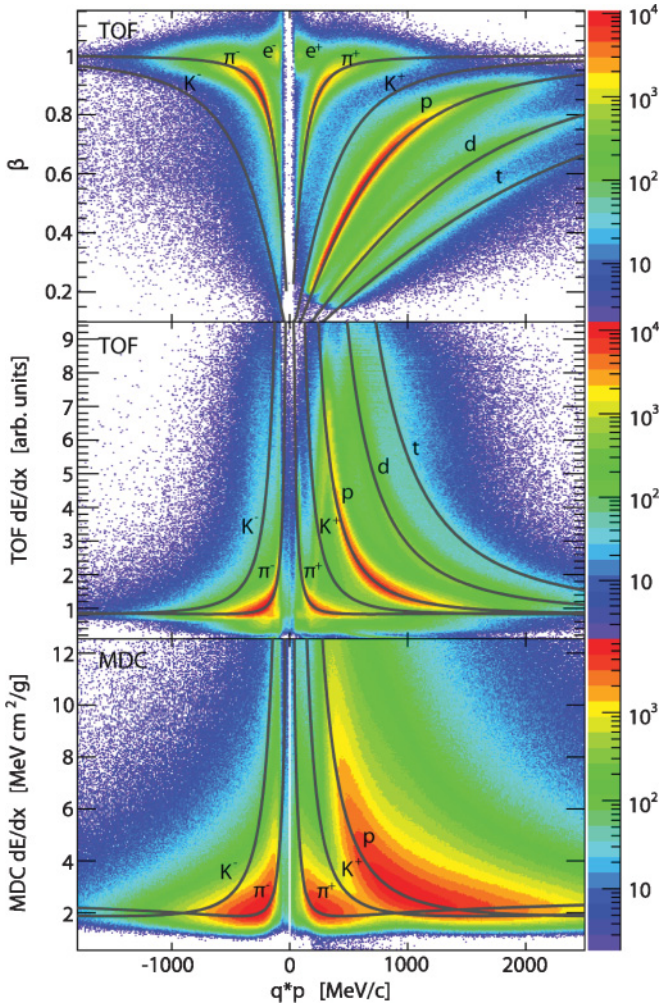

FIG. 1. (Color online) Particle velocity β (top, for the TOF detector) and dE/dx (middle for the TOF detector, bottom for the MDC) as a function of the momentum times the particle's polarity sign for the TOF detector.

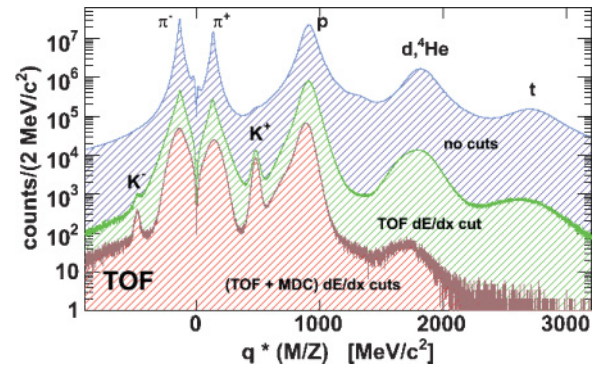

FIG. 2. (Color online) Polarity times mass over charge distributions for particle tracks measured in the TOF detector for different cut conditions. The spectrum on top (blue curve) shows the original distribution, whereas the lower two spectra show the effects of the graphical cuts in the TOF dE/dx (green histogram) and additionally the MDC dE/dx (red histogram) distributions, respectively.

velocity of light c) is determined by the time-of-flight between the diamond start detector and the corresponding hit in one of the two time-of-flight detectors and the reconstructed flight path. Figure 1 (top panel) shows the velocity β of the particles as a function of their polarity times momentum for the TOF system. Together with the experimental data, curves exploiting the relation $p = \beta\gamma m_0 c$, with m_0 as particle rest mass in vacuum and $\gamma = (1-\beta^2)^{-1/2}$, are shown for different particle species. The corresponding distribution for the TOFino system is not shown. It has a lower spatial and temporal resolution.

In addition to the arrival time, also the signal height is measured in TOF and TOFino. The latter one is proportional to the energy loss in the scintillators. The so-obtained distribution of the particle energy loss in the scintillator of the TOF system is shown in Fig. 1 (TOF dE/dx, center panel) as a function of polarity times momentum. The solid lines are obtained by fitting the Bethe-Bloch formula [41] to the proton distribution and then scaling the other curves according to the different particle masses. The separation power of this observable is comparable to the one obtained from the velocity measurement.

The bottom panel of Fig. 1 shows a similar distribution, but for the combined energy loss in the four MDCs of one sector. The energy-loss information is derived from the sense wire signals after unfolding effects due to the arrival time distribution of the drifting electrons that vary with track incident angle [37,39]. The solid curves in the same panel were calculated using the Bethe-Bloch formula. For the identification of $\pi^\pm$ and protons detected in the TOF, the β-versus-momentum information is used and the particles are selected by applying a graphical cut around the solid lines shown in Fig. 1 (top). The identification of $\pi^\pm$ and protons in the TOFino is performed in the same way, if the hit multiplicity per paddle is equal to 1; in the case of multiple hits, only the corresponding MDC dE/dx information is used to perform the selection.

For the $K^\pm$ identification, only the TOF data are considered, because of the rather large background in the TOFino due to its limited granularity and time resolution. As evident from Figs. 1 (top) and 2, the huge $\pi^\pm$ and proton background hides completely the $K^\pm$ signals. To reduce this background, graphical cuts based on calculated dE/dx distributions have been applied. The effect of these cuts on the signal-to-background ratio for the $K^\pm$ signal is exhibited in Fig. 2, where the application of the TOF dE/dx and the MDC dE/dx vs momentum selection reduces the background such that K^+ and K^- signals are clearly visible above the background.

C. K^+ and K^- spectra

Examples of the mass distribution obtained by applying both the TOF dE/dx and the MDC dE/dx cut are shown in Fig. 3. The data are shown in intervals of rapidity, $y = \frac{1}{2}\ln[(E+p_z)/(E-p_z)]$, and subtracted transverse mass $(m_t - m_{K^\pm}$ with $m_t = \sqrt{m_{K^\pm}^2 + p_t^2})$, where p_t, p_z, and E are the transverse and longitudinal momenta and the total energy of the particles, respectively. The solid lines in Fig. 3 correspond to a combined fit of the signal and background,

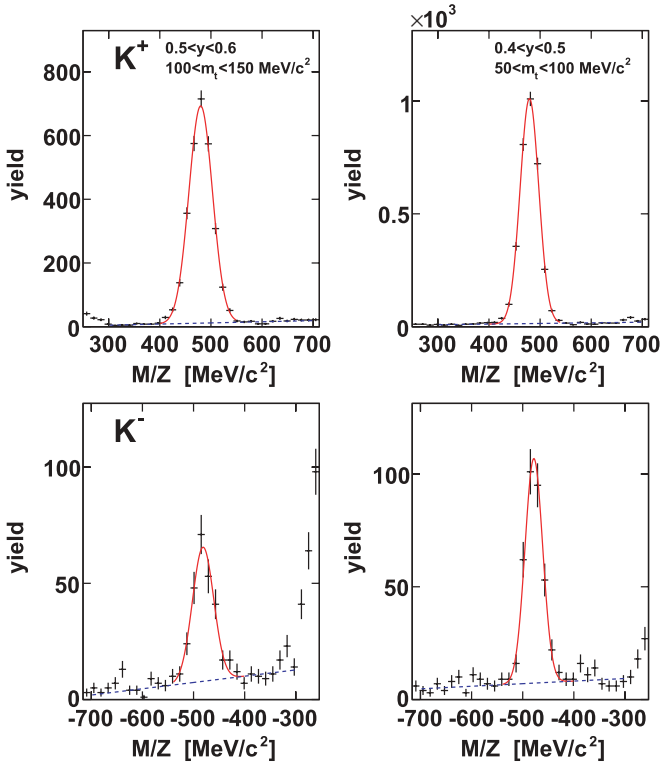

FIG. 3. (Color online) Reconstructed mass distributions of K^+ (top) and K^- mesons (bottom) for different phase space regions (left, $0.5 < y < 0.6$ and $100\,\mathrm{MeV}/c^2 < m_t < 150\,\mathrm{MeV}/c^2$; right, $0.4 < y < 0.5$ and $50\,\mathrm{MeV}/c^2 < m_t < 100\,\mathrm{MeV}/c^2$). The solid lines represent combined fits to the signal and background, whereas the dashed lines show the background part only.

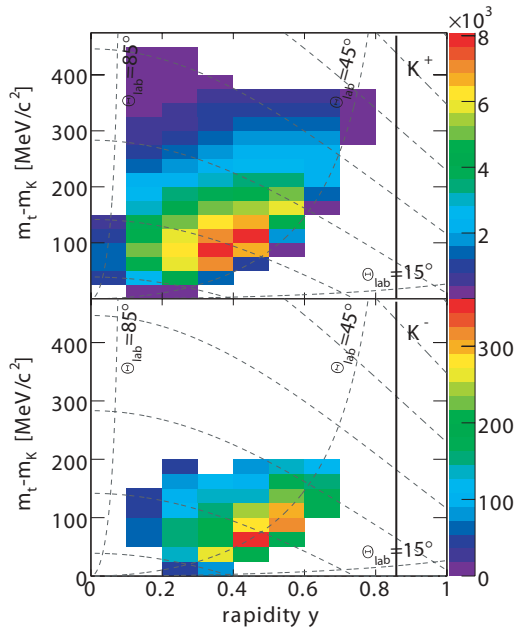

FIG. 4. (Color online) Distribution of measured K^+ (top) and K^- (bottom) yields in the TOF detector as a function of the subtracted transverse mass $m_t - m_{K^\pm}$ and the laboratory rapidity y. The color code refers to the counting rate. The dashed lines indicate the polar angles $\Theta = 15°$, $45°$, and $85°$ in the laboratory system. The dotted curves are for constant kaon momentum starting from $p = 200$ MeV/c in steps of 200 MeV/c. The vertical solid line depicts midrapidity.

while the dashed lines indicate the background. A Gaussian fit of the signal after the background subtraction and integrating over the whole covered phase space gives the following mean values and dispersions for the reconstructed masses: $\langle m_{K^\pm} \rangle = 485\,\mathrm{MeV}/c^2$ and $\sigma_{K^\pm} = 20\,\mathrm{MeV}/c^2$. The slight deviation of about 2% from the nominal rest mass of $m_K = 494\,\mathrm{MeV}/c^2$ [41] is attributed to imperfections in the time-of-flight calibration, to be improved for further analysis. Note, however, that all kinetic quantities are derived from the measured momentum while the time-of-flight serves for particle identification only. The signal-to-background ratio (S/B) for kaons depends on the location in phase space. It varies for K^+ mesons from 1.1 to 35.6 and for K^- mesons from 0.5 to 4.1.

The raw phase space distribution for the identified K^+ and K^- mesons after background subtraction is exhibited in Fig. 4, where the color code refers to the counting rate. Because of low statistics or large correction factors, mainly connected to the detector acceptance, not all of the shown bins are used in the further data analysis: only the rapidity bins between $0.1 < y_{\mathrm{LAB}} < 0.7$ have been considered. The three dashed lines in Fig. 4 refer to the laboratory polar angles of 18°, 45°, and 85°, respectively. The $K^\pm$ acceptance is limited to the TOF region $45° < \theta < 85°$.

D. Efficiencies

To extract quantitative information on the $K^\pm$ yields and momentum distributions over the whole phase space, acceptance and efficiency corrections must be applied. The total yields are finally obtained by extrapolating the measured phase space to 4π. The geometrical acceptance for K^+ and K^- has been determined as a function of the emission rapidity and transverse mass. A full-scale simulation of the HADES spectrometer was performed with the GEANT3 package [42]. Kaons and antikaons were generated with a flat (white) distribution in rapidity ($0 < y_{\mathrm{LAB}} < 0.7$) and transverse mass ($0\,\mathrm{MeV}/c^2 < m_t - m_K < 450\,\mathrm{MeV}/c^2$). Then the generated particles were propagated through the detectors and the resulting hits subjected to the selection criteria applied to the real data. The reconstruction efficiency was evaluated in two steps as a function of y and $m_t - m_K$. First, simulated K^+ and K^- tracks were embedded in real Ar + KCl experimental events and the single-track reconstruction efficiency was estimated. In a second step the PID efficiencies for $K^\pm$ were calculated using experimental data only, to reduce the systematic uncertainty introduced by the digitization. The efficiency of the TOF dE/dx and MDC dE/dx cuts was calculated by selecting a kaon sample using only one of the two cuts and estimating the reduction of the signal in the sample when the second cut is applied [43]. This procedure was applied for different rapidity and transverse mass intervals. The total reconstruction efficiency was obtained by multiplying the three components: track reconstruction, TOF dE/dx cuts,

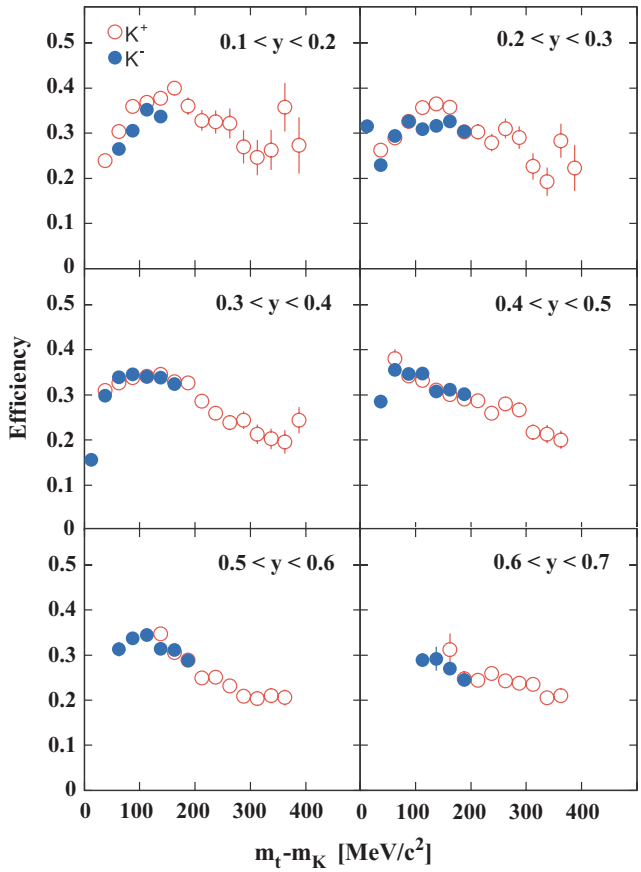

FIG. 5. (Color online) Reconstruction efficiency for K^+ and K^- as a function of the transverse mass for different rapidity intervals. The acceptances are not included (see text).

and MDC dE/dx cuts. Assuming that the efficiency for a given momentum slice is independent of the emission angle, the total efficiency was extrapolated also for the $y - m_t$ bins with low statistics. The reconstruction efficiency for K^+ and K^- was also estimated using only simulations, exploiting the embedded tracks method. The digitized data have been tuned such that the simulated dE/dx distributions of both MDC and TOF detectors reproduce the experimental distributions. The so-obtained efficiencies show a very good agreement (within 5%) with the efficiencies extracted from the experimental data and provide the basis for a realistic estimation of the systematic errors. The resulting efficiency is shown in Fig. 5 as a function of $m_t - m_K$ for different rapidity bins. These values do not include the acceptance, which varies from 20 to 40% for both particles analyzed only in the TOF region and in the four sectors equipped with four MDC planes each. The phase space coverage is displayed in Fig. 4.

E. ϕ mesons

To reconstruct ϕ mesons, K^+ and K^-, identified in both the TOF and TOFino systems and in all six sectors, are combined to pairs after the application of quality cuts that are more selective in the case of the TOFino detector.

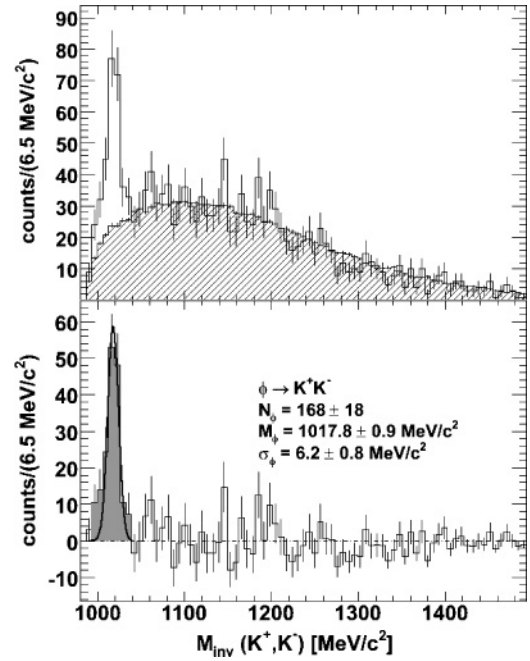

FIG. 6. (Color online) Invariant mass distribution of K^+-K^- pairs (top). The combinatorial background (shaded area) is obtained by the mixed-event technique. The background-subtracted distribution (bottom) shows a ϕ meson signal (grey area with a Gaussian fit) with a total yield of 168 ± 18 counts.

The resulting invariant mass distribution for the K^+-K^- pairs is shown in Fig. 6 (top) where the ϕ signal is clearly visible. Despite the fact that the kaon identification is more selective for the particles that hit the TOF detector than for those that hit the TOFino detector, the presence of the peak at the nominal ϕ mass with signal-to-background ratio better than 1 (see Fig. 6) shows that the purity of our selection is satisfactory for this investigation. Nevertheless, the continuum visible under the ϕ peak is contaminated with misidentified kaons and cannot be considered for quantitative conclusions on the K^+-K^- nonresonant pair yield. To extract the ϕ signal, the mixed-event technique was employed for the determination of the combinatorial background. Because a fourfold KCl target stack was used, only events in which the reaction took place in the same target segment were combined. The selection was done by calculating the minimal distance of the global event vertex with respect to the nominal target positions. Additionally, only events belonging to the same centrality class (MUL $\pm$ 4) were combined. The resulting combinatorial background distribution is shown by the hatched histogram in Fig. 6 (top), where the normalization has been obtained by scaling the mixed-event distribution to the same-event distribution (arithmetic sum) in the invariant mass region 1050–1400 MeV/c^2.

Figure 6 (bottom) shows the signal distribution after the background subtraction. We obtain for the reconstructed ϕ meson mass $m_\phi = (1017.8 \pm 0.9)$ MeV/c^2, a width of $\sigma_\phi = (6.2 \pm 0.8)$ MeV/c^2, and a total statistics of 168 ± 18 counts. To extract the geometrical acceptance and the reconstruction efficiency, a GEANT3 simulation of a "white" ϕ meson spectrum

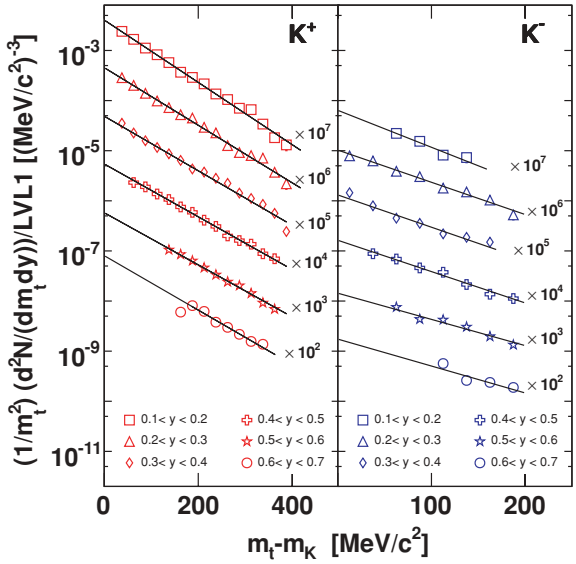

FIG. 7. (Color online) Invariant transverse mass spectra of reconstructed K^+ (left) and K^- (right) mesons. For the sake of clarity the spectra are plotted for several laboratory rapidity bins, see legends. The spectra are scaled by the factors as indicated in the plots.

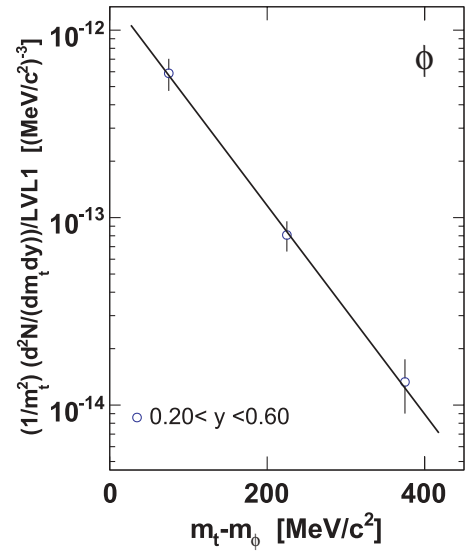

FIG. 8. (Color online) Invariant transverse mass spectrum of reconstructed ϕ mesons for the rapidity range $0.2 < y < 0.6$.

has been propagated through all the analysis steps. Each simulated K^+-K^- pair from a ϕ decay has been embedded in a real event to provide a realistic environment. The inclusive reconstruction efficiency for the ϕ meson has been evaluated to be about 1%. In addition the fraction of 90% of all ϕ is lost due to the acceptance and furthermore only 49.2% of all ϕ mesons decay into the channel K^+ or K^-, when using the free ϕ decay branching ratio.

IV. EXPERIMENTAL RESULTS

A. Transverse mass spectra

The invariant transverse mass spectra for K^+, K^-, and ϕ for different laboratory rapidity bins are exhibited in Figs. 7 and 8, respectively. These distributions were obtained by applying the efficiency correction to the raw data, including also the decay probability of each particle in channels that are not reconstructed in this analysis. The distributions show the number of counts per LVL1 trigger, per transverse mass and rapidity unit, divided by m_t^2. This representation is chosen to ease the comparison with a Boltzmann distribution. A fit according to

$$\frac{1}{m_t^2}\frac{d^2N}{dm_t dy} = C(y)\,\exp\left(-\frac{(m_t - m_0)c^2}{T_B(y)}\right) \qquad (1)$$

yields the solid straight lines shown in Figs. 7 and 8, which describe indeed the data quite well. The inverse slope of each distribution, $T_B(y)$, is shown in Fig. 9 as a function of the center-of-mass (c.m.) rapidity ($y_{\text{c.m.}} = y - y(\text{c.m.})$, where $y(\text{c.m.}) = 0.858$ for symmetric collisions at 1.756 GeV/nucleon) for K^+ (top) and K^- (bottom) mesons. The solid symbols display the measured data, whereas the open ones are reflected data with respect to the c.m. rapidity. The curves in Fig. 9 represent fits with

$$T_B(y) = \frac{T_{\text{eff}}}{\cosh(y)}, \qquad (2)$$

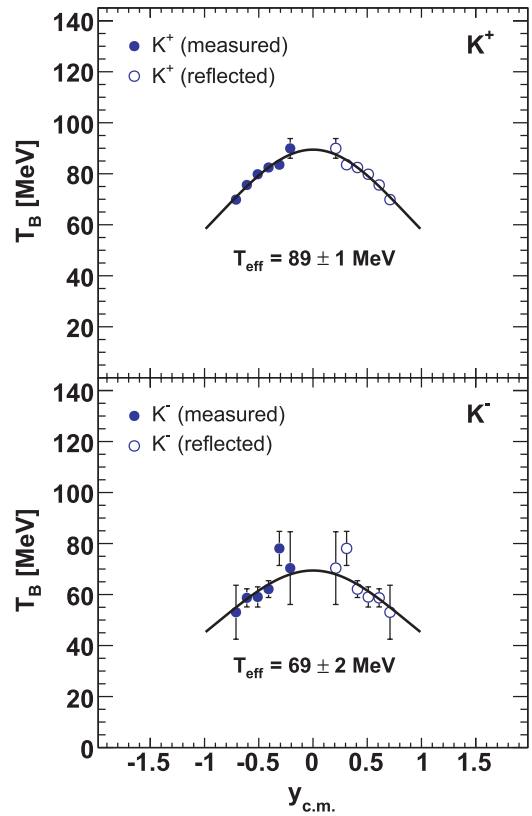

FIG. 9. (Color online) Rapidity dependence of the inverse slope parameters of K^+ (top) and K^- (bottom) mesons. The full symbols show the measured data, whereas the open ones are reflected data with respect to the c.m. rapidity. The lines represents fits with Eq. (2).

assuming a thermal source. The obtained parameter $T_{\rm eff}$ represents the inverse slope at midrapidity and may be considered as an effective temperature of the kinetic freeze-out of the respective particle. In particular, one can see from Fig. 9 that $T_{\rm eff}$ is lower for K^- than for K^+. This can be attributed to different freeze-out conditions for the two meson species [12].

B. Rapidity distributions

The fitted K^+ and K^- invariant transverse mass distributions $d^2N/(dm_t dy)$ in Fig. 7 are integrated within the interval $0 < m_t - m_K < \infty$ to obtain the meson yield per rapidity unit. A different approach to determine this integral is to integrate the measured data points and use the fits only for the extrapolation to the unmeasured phase space regions. However, the difference in yield to the method used is negligible. The resulting rapidity density distributions of K^+ and K^- are displayed in Fig. 10. The solid circles show the values calculated by the integration of Eq. (1), i.e., by means of

$$\left.\frac{dN}{dy}\right|_{y_i} = C(y_i)\left[(m_0c^2)^2 T_B(y_i) + 2m_0c^2 T_B^2(y_i) + 2T_B^3(y_i)\right]. \tag{3}$$

The parameters $T_B(y_i)$ and $C(y_i)$ are taken from the fits with Eq. (1) to the invariant transverse mass spectra. The open circles represent the reflection with respect to the center-of-mass rapidity. The rapidity density distributions have been fitted with Gaussian functions (solid curves represented in the two panels of Fig. 10). The distribution for K^+ has a width larger than that of the distribution for K^-, a fact which is also observed in other measurements [15].

In the fitting procedure, the center of the Gaussian was fixed at zero, taking into account the symmetry of the reaction. By integrating the fit function one obtains the kaon multiplicity per triggered event (LVL1). If the reflected points are included the extrapolation of the measured yield into the unmeasured rapidity region amounts to 35 and 31% of the determined total yield for K^+ and K^-, respectively. The resulting multiplicity values are collected in Table I. The first error following the multiplicity value indicates the statistical error. The evaluation of the systematic error is done in two steps. First, the graphical cuts on the MDC and TOF dE/dx distributions have been varied in width within 30% and the corresponding variation of the multiplicity has been calculated. This results in the first systematic error following the statistical one.

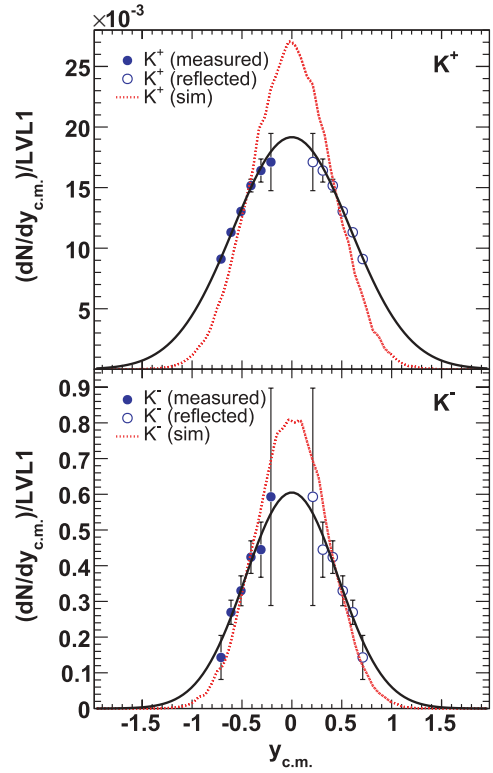

FIG. 10. (Color online) Rapidity density distributions of K^+ (top) and K^- (bottom) mesons. The solid symbols show the measured data, whereas the open ones are reflected data with respect to the c.m. rapidity. The curves represent Gaussian fits to the data. The overlayed dotted lines are simulated isotropic thermal distributions that have been normalized to the data (see text).

As shown in Fig. 10, the Gaussian parametrization of the data reproduces in a satisfactory way the experimental distribution. To check the sensitivity of the multiplicity results to the assumed parametrization, a double Gauss fit was also applied to the data following the procedure described in Ref. [44]. The resulting uncertainty on the kaon multiplicity is shown by the third error in Table I. The systematic error of the extracted inverse slope values has been estimated by varying the graphical cuts on the MDC and TOF dE/dx distribution within 30% as already mentioned above.

Figure 10 shows in addition to the experimental data and the Gauss fits the rapidity density distributions obtained from simulations of an isotropic thermal distribution of K^+ and

TABLE I. Total multiplicity/LVL1 and effective inverse slope parameters $T_{\rm eff}$ for K^+, K^-, and ϕ. The first error refers to statistical uncertainties, while the second and third errors represent the systematic ones, as described in the text. The fitted Gaussian width of the rapidity density distributions ($\sigma_{\rm exp}$) and the calculated width for a thermal and isotropic distribution ($\sigma_{\rm therm}$) of the corresponding effective temperature $T_{\rm eff}$ are also listed with systematic and statistical errors.

Particle	Multiplicity/LVL1	$\sigma_{\rm exp}$ ($y_{\rm c.m.}$)	$\sigma_{\rm therm}$ ($y_{\rm c.m.}$)	$T_{\rm eff}$
K^-	$(7.1 \pm 1.5 \pm 0.3 \pm 0.1) \cdot 10^{-4}$	0.465 ± 0.0565	0.374 ± 0.024	$69 \pm 2 \pm 4$
K^+	$(2.8 \pm 0.2 \pm 0.1 \pm 0.1) \cdot 10^{-2}$	0.586 ± 0.0223	0.425 ± 0.011	$89 \pm 1 \pm 2$
ϕ	$(2.6 \pm 0.7 \pm 0.1^{+0.0}_{-0.3}) \cdot 10^{-4}$	—	0.287 ± 0.027	84 ± 8

K^-, respectively. The simulated distributions are represented by the dotted lines in the upper and lower panels of Fig. 10 and are normalized to the total integral of the experimental ones. The measured distributions are systematically wider than the simulated ones (see Table I). For K^+ the increase in width is larger and amounts to roughly 30%.

Deviations from a thermal picture of a particle emitting source are due to anisotropies of the angular and/or of the momentum distributions. The limited acceptance of the HADES detector precludes such a differentiation at the current stage of analysis.

The rapidity density distribution of the measured ϕ mesons contains only one data point. Therefore, one must fix the width of the distribution to estimate the ϕ multiplicity. If a thermal description of the rapidity density distribution is assumed, its width σ_y can be calculated according to

$$\sigma_y = \sqrt{\frac{T_{\text{eff}}}{m_\phi c^2}}, \tag{4}$$

where T_{eff} represents the effective inverse slope for ϕ mesons. This parameter is calculated taking the inverse slope T_B obtained in fitting the invariant transverse mass distribution of the ϕ meson for the rapidity bin shown in Fig. 8 and substituting this value into Eq. (2).

Table I shows the total ϕ meson multiplicity per triggered event (LVL1) obtained by integrating the so-obtained Gaussian curve. The first error shown is again purely statistical. Because of the extended rapidity bin chosen for the ϕ mesons the change of the yield within the bin is not negligible. Instead of using the center rapidity of this bin we take a value weighted with the expected thermal distribution across the bin width. This procedure reduces the extrapolated total yield by around 24% compared to an extrapolation where the rapidity point is in the center of the bin. The systematical error estimated for the total ϕ multiplicity/LVL1 shown in Table I is obtained by varying the temperature T_{eff} within its statistical error.

Existing theoretical calculations assume an isotropic emission of the ϕ meson [38,45,46], but because the angular distribution of the emitted ϕ has not yet been measured at these energies, an additional source of systematical error must be considered. On the basis of the previously mentioned maximal deviation of the K^+ rapidity distribution from an isotropic source, we assume 30% to be the maximum error in the evaluation of the width of the rapidity distribution for the ϕ meson. This translates into a second systematic error for the ϕ multiplicity/LVL1, which is also presented in Table I. This has been calculated assuming a larger width of the ϕ rapidity density function and hence leads to an asymmetric error.

The value of the effective temperature of the ϕ meson is shown as well in Table I together with its statistical error.

V. DISCUSSION

Let us first compare our data with results recently published by the KaoS Collaboration [15]. If the K^-/K^+ multiplicity ratio is plotted as a function of the beam energy for the inclusive data and for various systems measured by KaoS [15,47], as shown in Fig. 11, one can see that the ratio increases with beam energy and that the HADES data point fits nicely into the energy systematics.

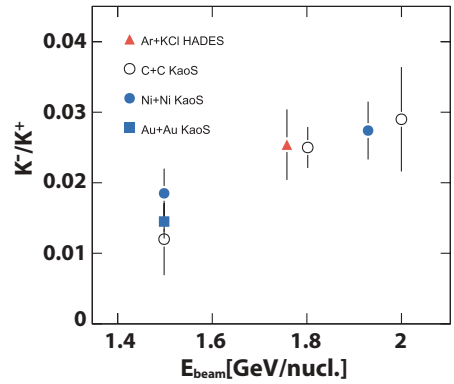

FIG. 11. (Color online) K^-/K^+ ratios as a function of the kinetic beam energy for various systems. The present HADES data point is depicted by the solid triangle. KaoS data are from Ref. [15].

In Fig. 12 the centrality dependence of the K^-/K^+ ratio is exhibited for the Au + Au and Ni + Ni systems and for two different beam energies. As a measure of the centrality, the number of participants A_{part} is chosen. This quantity is calculated within a geometrical model of interpenetrating spheres where the impact parameter range is derived from a comparison of the charged particle multiplicities, as measured in the TOF/TOFino detectors, to that provided by GEANT predictions with the UrQMD transport model [48] as event generator. The solid triangle represents the data point measured for Ar + KCl at 1.756 GeV/nucleon in the present experiment. For the LVL1 trigger we attribute to our data a value of $A_{\text{part}} = 38.5 \pm 4$, being about twice the minimum bias value. Our data point fits well into the systematics when taking into account the beam energy dependence. Looking at the open squares (Ni + Ni at 1.5 GeV/nucleon) and solid squares (Au + Au at

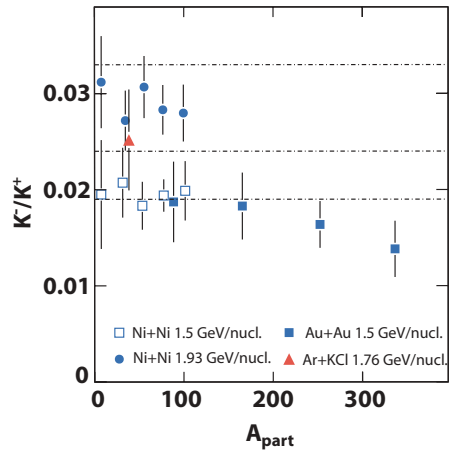

FIG. 12. (Color online) A_{part} dependence of the K^-/K^+ ratio for different beam energies and colliding systems. The solid triangle depicts the present HADES data. The other symbols display KaoS results from Ref. [15]. The dashed lines show the prediction of a thermal model [49,50] for kinetic beam energies of 1.5, 1.76, and 1.93 GeV/nucleon (from bottom to top).

1.5 GeV/nucleon), it can be seen that the ratio stays fairly constant with $A_{\rm part}$, supporting our implicit assumption on the centrality independence in using an averaged value of $A_{\rm part}$. Together with the data, K^-/K^+ ratios predicted by the thermal model [49,50] are shown for kinetic beam energies of 1.5, 1.76, and 1.93 GeV/nucleon. These calculated values are found to be in fair agreement with the experimental values. The fact that the ratio K^-/K^+ does not depend noticeably on the centrality of the reaction and that the meson yield is consistent with the prediction of thermal models has been used in the past to support the hypothesis that most of the K^- are produced in multistep processes like

$$NN \rightarrow YK^+N, \quad E_{\rm th} = 1.58\,{\rm GeV}, \tag{5}$$

$$Y\pi \leftrightarrow NK^-, \tag{6}$$

where Y stands for the hyperons Λ and Σ, and $E_{\rm th}$ denotes the beam energy threshold in free nucleon-nucleon collisions. Equation (6) is called strangeness exchange. The dependence of the K^+ and K^- multiplicities on $A_{\rm part}$ has been found to be quite smooth [15]: $m_{K^+} \propto A_{\rm part}^{\alpha}$, with $\alpha_{K^+}(Ni) = 1.26 \pm 0.06$; and $m_{K^-} \propto A_{\rm part}^{\alpha}$, with $\alpha_{K^-}(Ni) = 1.25 \pm 0.12$. (In contrast, the $\pi^{\pm}$ multiplicity is found to linearly dependent on $A_{\rm part}$, $\alpha = 1$). Along these considerations it has been claimed in Ref. [49] that Eq. (6) is the dominant channel for K^- production.

Further possible channels for the production of K^- in nucleon-nucleon collisions are

$$NN \rightarrow \phi NN \rightarrow K^+K^-NN, \quad E_{\rm th} = 2.59\,{\rm GeV}, \tag{7}$$

$$NN \rightarrow K^+K^-NN, \quad E_{\rm th} = 2.49\,{\rm GeV}, \tag{8}$$

with thresholds being higher than those for the previous reaction.

The threshold for production induced by a Δ resonance $N\Delta \rightarrow K^+K^-NN$ depends on the mass (energy) of the resonance, but it is comparable to the value quoted in Eqs. (7) and (8). Further secondary collisions have been considered in Refs. [38,45,46] to contribute to the ϕ production, such as $\pi N \rightarrow \phi N$, $\pi N(1520) \rightarrow \phi N$, $\rho N \rightarrow \phi N$, $\rho\Delta \rightarrow \phi N$, and $\pi\rho \rightarrow \phi$. It must be pointed out [38,45,46] that the predicted ϕ multiplicity in subthreshold heavy-ion collisions, calculated including all the channels mentioned above, stay below the number extracted from the experimental data in Ref. [20].

The newly measured HADES data provide, for the first time at SIS energies, a consistent measurement of K^+, K^-, and ϕ in the same data sample. The ϕ/K^- ratio measured with the HADES spectrometer for Ar + KCl at 1.756 GeV/nucleon is found to be 0.37 ± 0.13 (see Table I). This value translates into a fraction of $18 \pm 7\%$ of K^- coming from ϕ decay. This implies that also below threshold the ϕ production contributes significantly to the K^- rate, as already argued in Ref. [38]. By taking for the ϕ meson the decay path $c\tau \approx 46$ fm as follows from the vacuum width, one can estimate a fraction of about 80% decaying outside the collision zone, for which we employ a radius of about 10 fm. The question of the in-medium width of the ϕ meson is certainly far from being settled, because the few available data do not yet deliver a consistent picture [51]. However, if we assume that a large amount of $\phi \rightarrow K^-K^+$ decays would take place in the fireball volume, because of the strong interaction experienced by kaons in medium, the resulting signal in the K^-K^+ invariant mass spectrum would be washed out. Hence, K^- stemming from ϕ decays reconstructed in this analysis are produced mostly outside the medium. This effect will also dilute any observed medium effects of K^-. To extract precise information on the equation of state [8–10] and on the K^--nucleon potential, one should improve the statistics of such independent measurements for K^- and ϕ, i.e., tag K^- mesons according to their production mechanism. This kind of systematic measurements should be done for different systems and different beam energies.

To understand quantitatively the role of the strangeness exchange mechanism for the production of K^-, the creation mechanism of the hyperons involved in the process deserves further studies. The rapidity and transverse momentum distribution of Λ hyperons produced in the Ar + KCl reaction at 1.756 GeV/nucleon will be made available soon.

Also the nonresonant K^+-K^- production [say by the reaction Eq. (8)] plays an important role in $p + p$ reactions, contributing to about 50% of the overall K^+-K^- yield [27]. This contribution is not yet known in heavy-ion collisions, because the K^+-K^- invariant mass spectrum measured by HADES still contains a non-negligible contribution of fake candidates [see discussion of Fig. (8)]. If one assumes that the contribution of the nonresonant K^+-K^- production in Ar + KCl at 1.756 GeV/nucleon is comparable with the value measured for $p + p$ at 2.7 GeV [27], taking the ratio ϕ/K^- measured by HADES, it can be estimated that about 38% of all produced K^- mesons do not stem from strangeness exchange reactions but from the sum of resonant and nonresonant K^+-K^- production [Eqs. (7), (8)].

This consideration further deprives the strangeness exchange mechanism of its leading role in the K^- production in subthreshold heavy-ion reactions.

In Fig. 13, the ϕ/K^- ratio measured by HADES is compared to the ratios measured at higher energies in Pb + Pb [52] and Au + Au collisions [53,54] and in $p + p$ reactions at 2.7 GeV [27]. For heavy-ion collisions one can see that, while the ratio is rather constant at high energies, it is substantially larger in the case of the HADES measurement.

The various curves in Fig. 13 show the predictions by the statistical model for four different values of the correlation length R_C [49]. This parameter is the radius of the volume inside which the production of particles with open strangeness is canonically conserved in the calculation. One can see that a value of R_C between 2.2 and 3.2 fm is needed to fit the prediction by the statistical model [49] to the HADES result. This value of R_C translates into a reduced volume for local strangeness production and conservation. The fact that the HADES result is consistent with a somewhat smaller volume with respect to the other results could be interpreted as a hint that the contribution to K^- production by strangeness exchange, which is more probable for larger volumes, is diminished in the SIS energy regime.

As also shown in Fig. 13, the ϕ/K^- ratio measured in elementary reactions is found to be consistent with a calculation using $R_C = 1.2$ fm, but this curve fails to join the others ($R_C = 2.2$, 3.2, and 4.2 fm) at higher $\sqrt{s_{NN}}$ values.

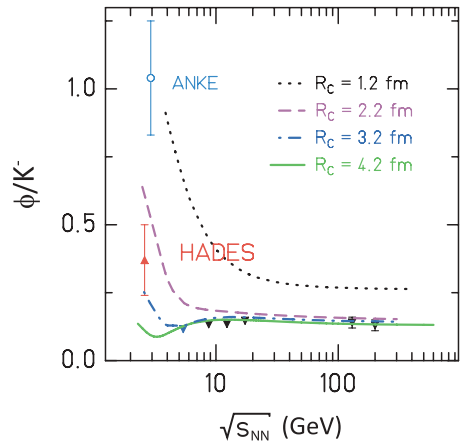

FIG. 13. (Color online) ϕ/K^- ratio as a function of center-of-mass energy $\sqrt{s_{NN}}$. The solid triangle on the left shows the HADES point, whereas the other data points represented by solid triangles refer to results from heavy-ion measurements at higher incident energies [52–54]. The open circle presents the value measured in $p+p$ at 2.7 GeV [27]. The lines are predictions of a statistical model [49,50] for four parameters of the correlation radius R_C.

The fact that the ratio measured by HADES is smaller than the one extracted for $p+p$ reactions tight above threshold shows the role played by secondary processes in the K^- production in subthreshold heavy-ion collisions. However, if the strangeness exchange process were the dominant mechanism for K^- production, the ϕ/K^- ratio would be much smaller than the measured value.

VI. SUMMARY

In summary, we report on a first measurement of charged kaons and the ϕ meson production in the same experiment at SIS energies. The HADES data on $K^\pm$ fit well into the systematics of the results published by the KaoS Collaboration. The K^-/K^+ ratio is consistent with the value predicted by the thermal model. The effective inverse slope parameters of K^+ and K^- are determined; the inverse slope of K^+ mesons is found to be higher than that for K^- mesons, in agreement with the KaoS data.

The ϕ/K^- ratio has been deduced from our data with improved accuracy as compared with previous measurements. The HADES value was found to be 0.37 ± 0.13, translating into a fraction of $18 \pm 7\%$ of K^- stemming from ϕ decays. Because the ϕ decays that can be measured via the invariant mass reconstruction of K^+-K^- pairs are essentially those happening outside the nuclear medium, this value may be considered as a lower limit. However, the nonresonant K^+-K^- production may also play an important role for the total K^- yield, but to draw quantitative conclusions the purity of the kaon identification in heavy-ion reactions must be improved.

Furthermore, high statistics measurements are necessary to tag and distinguish the K^- coming from the ϕ decay from those stemming from nonresonant processes. In this way, a quantitative comparison of this process in heavy-ion and pp reaction can be carried out. The contribution of the ϕ meson to the K^- production in heavy-ion collisions could be further enhanced by the violation of the OZI restriction. Results of the ϕ/ω ratio measured in the di-electron decay channel in Ar + KCl by HADES will be soon made available and deliver further information on this item.

In general it can be concluded that for heavy-ion collisions at beam energies below the free ϕ production threshold, the K^- production cannot be explained exclusively by the strangeness exchange mechanism. Furthermore, the ϕ/K^- ratio for the Ar + KCl system has been compared to the ratio measured in heavy-ion collisions at higher energies and to the ratio extracted from $p+p$ reactions at 2.7 GeV. The ϕ/K^- ratio measured by HADES has been found to be higher than the almost constant value found at higher energies. The correlation parameter $R_C \leqslant 3.2$ fm must be used in the calculation by the statistical model to reproduce the HADES measurement. This value is lower than the one used to fit the ϕ/K^- measured in heavy-ion collisions at higher energies. A reduced value of R_C can be interpreted as a reduced volume in which strangeness production and conservation are taking place. This reduced volume might lead to a less significant contribution of the strangeness exchange mechanism to the K^- production, which is more probable for larger volumes.

The contribution of the different secondary processes to the total K^- is visible in the difference between the ϕ/K^- ratio measured in $p+p$ reactions at 2.7 GeV and in Ar + KCl collisions at 1.756 GeV/nucleon. The observed relative high ratio measured by HADES seems to deprive the strangeness exchange mechanism of its dominant contribution to K^- production, as stressed above.

It is clear that, to extract an excitation function, further systematic measurements of the ϕ and K^- production must be performed. HADES is a suitable apparatus for this kind of study, especially due to its capability to reconstruct the ϕ not only via the charged kaon decay but also via the direct electromagnetic decay into lepton pairs. Because leptons do not undergo strong interactions and therefore are able to leave the reaction zone nearly undisturbed, one will be able to distinguish between those ϕ mesons that decay inside the medium and those that decay outside. This will provide an observable directly sensitive to the predicted medium modifications.

ACKNOWLEDGMENTS

We gratefully acknowledge the useful discussions with H. Oeschler and K. Redlich. In particular we thank K. Redlich for providing the calculations by the statistical model. The HADES Collaboration gratefully acknowledges support from the following: BMBF Grants 06TM970I, 06GI146I, 06F-140, and 06DR135 (Germany); GSI (TM-FR1, GI/ME3, OF/STR); Excellence Cluster of Universe (Germany); Grants GA AS CR IAA100480803 and MSMT LC 07050 (Czech Republic); Grant KBN 5P03B 140 20 (Poland); INFN (Italy); CNRS/IN2P3 (France); Grants MCYT FPA2000-2041-C02-02 and XUGA PGID T02PXIC20605PN (Spain); Grant UCY-10.3.11.12 (Cyprus); INTAS Grant 06-1000012-8861; and EU Contract RII3-CT-2004-506078.

[1] D. B. Kaplan and A. E. Nelson, Phys. Lett. **B175**, 57 (1986).
[2] G. Brown, C. H. Lee, M. Rho, and V. Thorsson, Nucl. Phys. **A567**, 937 (1994).
[3] C. Hartnack, J. Jaenicke, L. Sehn, H. Stöcker, and J. Aichelin, Nucl. Phys. **A580**, 643 (1994).
[4] E. E. Kolomeitsev, D. N. Voskresenski, and B. Kämpfer, Nucl. Phys. **A588**, 889 (1995).
[5] T. Waas, N. Kaiser, and W. Weise, Phys. Lett. **B379**, 34 (1996).
[6] J. Schaffner-Bielich, J. Bondorf, and A. Mishustin, Nucl. Phys. **A625**, 325 (1997).
[7] M. Lutz, Phys. Lett. **B426**, 12 (1998).
[8] C. M. Ko and G. Q. Li, J. Phys. G **22**, 1673 (1996).
[9] G. Q. Li, C.-H. Lee, and G. E. Brown, Nucl. Phys. **A625**, 372 (1997).
[10] W. Cassing, E. L. Bratkovskaya, U. Mosel, S. Teis, and A. Sibirtsev, Nucl. Phys. **A614**, 415 (1997).
[11] C. Sturm *et al.* (KaoS Collaboration), Phys. Rev. Lett. **86**, 39 (2001).
[12] A. Förster *et al.* (KaoS Collaboration), Phys. Rev. Lett. **91**, 152301 (2003).
[13] P. Senger, Prog. Part. Nucl. Phys. **53**, 1 (2004).
[14] F. Uhlig *et al.* (KaoS Collaboration), Phys. Rev. Lett. **95**, 012301 (2005).
[15] A. Förster *et al.* (KaoS Collaboration), Phys. Rev. C **75**, 024906 (2007).
[16] J. L. Ritman *et al.* (FOPI Collaboration), Z. Phys. A **352**, 355 (1995).
[17] D. Best *et al.* (FOPI Collaboration), Nucl. Phys. **A625**, 307 (1997).
[18] K. Wisniewski *et al.* (FOPI Collaboration), Eur. Phys. J. A **9**, 515 (2000).
[19] P. Crochet *et al.* (FOPI Collaboration), Phys. Lett. **B486**, 6 (2000).
[20] A. Mangiarotti *et al.* (FOPI Collaboration), Nucl. Phys. **A714**, 89 (2003).
[21] S. Schnetzer *et al.*, Phys. Rev. Lett. **49**, 989 (1982); Phys. Rev. C **40**, 640 (1989).
[22] W. Scheinast *et al.* (KaoS Collaboration), Phys. Rev. Lett. **96**, 072301 (2006).
[23] S. Barsov *et al.* (ANKE Collaboration), AIP Conf. Proc. **549**, 421 (2002).
[24] P. Winter *et al.* (COSY-11 Collaboration), Phys. Lett. **B635**, 23 (2006).
[25] S. Abd and El-Samadh *et al.* (TOF Collaboration), Phys. Lett. **B632**, 27 (2006).
[26] M. Hartmann *et al.* (ANKE Collaboration), Phys. Rev. Lett. **96**, 242301 (2006).
[27] Y. Maeda *et al.* (ANKE Collaboration), Phys. Rev. C **77**, 015204 (2008).
[28] Y. Shin *et al.* (KaoS Collaboration), Phys. Rev. Lett. **81**, 1576 (1998).
[29] G. Q. Li *et al.*, Phys. Lett. **B381**, 17 (1996).
[30] E. Bratkovskaya *et al.*, Nucl. Phys. **A622**, 593 (1997).
[31] C. Fuchs, A. Faessler, E. Zabrodin, and Y. M. Zheng, Phys. Rev. Lett. **86**, 1974 (2001).
[32] C. Hartnack and J. Aichelin, J. Phys. G **28**, 1649 (2002).
[33] C. Hartnack, H. Oeschler, and J. Aichelin, Phys. Rev. Lett. **90**, 102302 (2003).
[34] C. Fuchs, Prog. Part. Nucl. Phys. **56**, 1 (2006).
[35] G. Agakichiev *et al.* (HADES Collaboration), arXiv:nucl-exp/0902.3478v1; R. Schicker *et al.*, Nucl. Instrum. Methods A **380**, 586 (1996); P. Salabura *et al.* (HADES Collaboration), Nucl. Phys. **A749**, 150 (2005).
[36] G. Agakichiev *et al.* (HADES Collaboration), Phys. Rev. Lett. **98**, 052302 (2007).
[37] A. Schmah, Doctoral thesis, Darmstadt, 2008.
[38] B. Kämpfer, R. Kotte, C. Hartnack, and J. Aichelin, J. Phys. G **28**, 2035 (2002).
[39] J. Markert, Doctoral thesis, Frankfurt, 2005.
[40] A. Sadovsky, Doctoral thesis, Dresden, 2007.
[41] W.-M. Yao *et al.*, J. Phys. G **33**, 1 (2006).
[42] GEANT 3.21, Detector Description and Simulation Tool, http://consult.cern.ch/writeup/geant/, 1993.
[43] M. Lorenz, Diploma thesis, Frankfurt, 2008.
[44] C. Alt *et al.*, Phys. Rev. C **78**, 044907 (2008).
[45] M. Zetenyi *et al.*, J. Phys. G **28**, 2133 (2002).
[46] H. W. Barz *et al.*, Nucl. Phys. **A705**, 223 (2002).
[47] A. Förster *et al.* (KaoS Collaboration), J. Phys. G **31**, 693 (2005).
[48] S. A. Bass *et al.*, Prog. Part. Nucl. Phys. **41**, 255 (1998); M. Bleicher *et al.*, J. Phys. G **25**, 1859 (1999).
[49] J. Cleymans, A. Förster, H. Oeschler, K. Redlich, and F. Uhlig, Phys. Lett. **B603**, 146 (2004).
[50] K. Redlich (private communication).
[51] V. Metag, Prog. Part. Nucl. Phys. **61**, 245 (2008).
[52] S. V. Afanasiev *et al.* (NA49 Collaboration), Phys. Lett. **B491**, 59 (2000).
[53] J. Adams *et al.* (STAR Collaboration), Phys. Lett. **B612**, 181 (2005).
[54] B. Holzman *et al.* (E917 Collaboration), Nucl. Phys. **A698**, 643 (2002).